Development of a zoom probe for spatially resolved diffuse transmittance studies.

Master Thesis

by

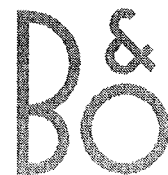Anders Becker

LUND
UNIVERSITY

BANG & OLUFSEN

1. Abstract

A zoom probe for spatial resolved measurements of tissue optical properties was developed and evaluated. The zoom probe is a flexible research equipment that will be used to evaluate how a commercial product should be designed to give the best results at the lowest possible cost. This thesis covers a large part of the development of this equipment. It includes the theoretical studies how the zoom probe should be designed to be able to examine the desired biological media, as well as the practical work of setting up the equipment aligning, calibrating etc. Theoretical studies based on Monte Carlo simulations are made as a way to solve the inverse problem of determining the optical properties. We also have a brief discussion of the problems that can occur when using a thin cuvette and a sample with a small scattering coefficient. Finally, some trial measurements are done on latex spheres to evaluate the performance of the zoom probe.

2. Introduction

This thesis deals with the construction of a zoom probe for spatially resolved measurements of tissue optical properties. Tissue optical properties are essential in all medical laser applications when trying to describe the way in which light propagates through tissue. Knowledge about light propagation is important when you want to know to what depth a treatment reaches or for calculating the given dosage. Moreover, tissue optical properties can be used in a more direct way to give information of the tissue or sample you are looking at.

When light hits a small particle the light will be affected and its direction of motion will be changed; the light is scattered. By studying the scattered light from many such scattering events, we can get knowledge about the particles in a media, $e.g.$ size and shape [1]. However, in most biological cases the concentration of scatterers are so high that the once scattered light will be scattered again and again before we can detect it, we have multiple scattered light. The optical properties μ_s and μ_a of a media correspond to the reciprocal of the mean distance a photon will travel in the media before it is scattered or absorbed. The optical property g describes the probability that the light will be scattered in a certain direction. The optical properties are thereby only valid in a macroscopic sense. By studying the spatial distribution of the multiple scattered light, $i.e.$ the scattering profile, we can draw conclusions of what the optical properties of the media are [2]. If we simplify our model, we can say that the things that affect the optical properties are the difference between the refractive index of the scatterers and the refractive index of the surrounding media. We also have to take into account the size and concentration of the scatterers and the concentration of absorbers to calculate the optical properties correctly. Some natural biological molecules, e.g. glucose, can give a recognisable pattern for us to be able to determine the concentration level in the body [8]. This effect is caused by that, an increased glucose level in the blood leads to increased refractive index of the surrounding media. This will yield less difference between the refractive index of the media and the cellular structures, thus lower scattering coefficient. Nevertheless, in many cases, this method is not enough and it is necessary to take an extra step to be able to resolve the concentration of a certain molecule. One such case is in CRP-analysis (C-reactive protein), were a certain chemical is mixed with a blood plasma sample in $vitro$. The chemical reacts with the CRP in the blood and creates aggregates, which are large enough to dominate the scattering. The concentration of CRP-aggregates can then be measured and out of that, one can draw conclusions about the concentration of CRP in the blood. CRP is only present in low concentrations in healthy individuals but if the patient has an infection in his body an increase of the patient's CRP-level is noticed [3]. Due to this ability, many physicians use CRP-analysis as one of the most common tests to check for infection.

This project is a co-operative project between Lund University Medical Laser Centre (LMLC) and Bang & Olufsen Medicom A/S. LMLC has a long experience in understanding light propagation in biological media, whereas B&O Medicom are a technology company interested in the development of minimal and non-invasive diagnostic instruments for use in a doctor's office or in the homecare market. For B&O to reach that goal, extensive studies are made to determine how such products should be designed. The zoom probe is a part of this evaluation project. It is built to be flexible

and adaptable to make it easy to evaluate different set-ups of the system and for optimising the set-up for looking at different biological media. There are certain advantages in measuring optical properties with the zoom probe compared with other methods, *e.g.* radial distributed optical fibres or CCD-detector [4]. The zoom probe has the zooming and non-contact quality of a CCD-detector, combined with the high dynamic range and the high signal-to-noise ratio of a silicon photodiode.

To be able to analyse the data the zoom probe is acquiring, we simulate the scattering processes using Monte Carlo simulations for different relevant optical properties. For solving the inverse problem, to extract the optical properties from our set of measured data, we are using a multivariate data analyse method [2].

3. Theory

3.1 Absorption and scattering of light by small particles

Generally speaking, light can interact with a media in two ways; it can be absorbed or it can be scattered. In this section we will study these different events in the microscopic sense. This means that we only study how a photon is affected by one scattering event. In addition, we do not study the cases where the photon changes energy as in Raman scattering or as when a photon is emitted by fluorescence.

3.1.1 Scattering

When looking at the microscopic case of scattering it is easiest to look at light as electromagnetic waves. All matter consists of electric charges, protons and electrons, so when an electromagnetic wave interacts with a particle the electric charges in the particle are influenced by the electromagnetic wave (EM-wave) and the particle becomes an oscillating dipole. The dipole is oscillating with the same frequency as the incident wave. An oscillating dipole works like an antenna and radiate electromagnetic energy in all directions except the direction of the oscillation. This re-radiated electromagnetic wave is called scattered light. When electromagnetic wave hits a particle it doesn't just create one dipole, it induces many dipoles in different regions of the particle [4].
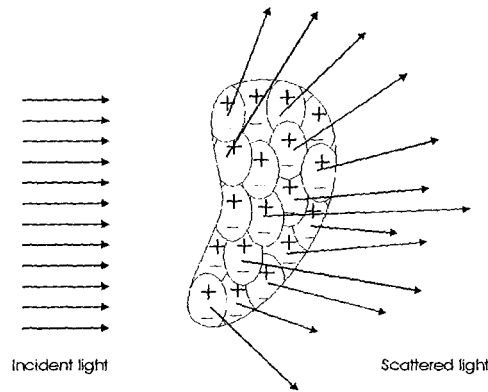

Incident light   Scattered light

Figure 3.1 The electromagnetic wave induces dipoles in the particle, the dipole regions reemitts the EM-wave in all directions.

All these dipoles reemit scattered light and the total light scattered by the particle is acquired by superposing the scattered light from all regions taking to account the phase differences. Due to the phase differences, the total amount of scattered light will vary with the scattering direction. This angular scattering distribution is often called the phase function. For a small particle, with size less than the wavelength of the incident beam, all the dipole regions will be close to each other and phase differences will be small which leads to isotropic scattering, so called Rayleigh scattering. However, if the particle is big compared to the wavelength, the phase differences become big enough to cancel out certain areas of the angular distribution and enhance others. This will lead to a more complex phase function. For a big particle, the shape of the particle will also

affect the phase function, so by studying the angular scattering distribution of a scattering experiment, one can draw conclusions regarding the particles size and shape.

3.1.2 Absorption

The energy of the electromagnetic wave doesn't have to be re-radiated, it can be absorbed and its energy transformed into some other form of energy, *e.g.* thermal energy. Which wavelengths that are absorbed and with what efficiency differ is depending on the energy state structure of the molecule.

3.2 Mie theory

As stated before, when $\lambda \gg$ size of the scatterer we have Rayleigh scattering. Geometrical optics works as a good approximation to the electromagnetic theory when the objects are sufficiently large, $\lambda \ll$ size of the scatterer. However, for smaller objects in the region where $\lambda \approx$ size of scatterer, geometrical optics fails to be valid. Fortunately, for spherical scatterers we are able to solve Maxwell's equations to describe the physics of how the electromagnetic wave interacts with the sphere, this is known as Mie theory [6]. The Mie theory gives us a tool to calculate the absorption and scattering cross sections as well as the angle-dependent scattering function. From these properties, we can derive the absorption and scattering coefficient as well as the anisotropy factor. These coefficients are used to characterise the multiple scattering described in the next section.

3.3 Transport theory

For the case of a single sphere, we are able to solve Maxwell's equations. However, in the more complex case of biological media, it is an almost impossible task to know the distribution of the dielectric properties within the media. Moreover, even if the dielectric properties were known these equations would be almost impossible to solve due to the great number of contributing factors. Therefore, we need another approach. Instead of treating the light as electromagnetic waves we can treat the light as a stream of particles, photons. This approach is known as transport theory [7]. It is valid in a statistical sense, averaging all interaction events taking place in the media. The theory is based on studying the incoming, outgoing, absorbed and emitted photons in an infinitesimal volume element in the media. We assume that the scatterers and absorbers in the media are small and uniformly distributed throughout the material. We let the properties of the tissue be represented by three parameters, the absorption coefficient, μ_a and scattering coefficient, μ_s and the anisotropy factor, g.

3.3.1 Absorption and scattering coefficients

Absorption and scattering coefficients are defined as the probability for absorption/scattering of a photon per unit path length and have the dimension [length^{-1}]. A photon travelling a small distance ds has the probability of $\mu_s ds$ that it will be scattered and correspondingly for absorption.

10

3.3.2 Anisotropy factor

When we have a scattering event the phase function, $p(\cos\theta)$, describes the probability that the light will be scattered in certain angle θ in the range 0 to π. In tissue optics, this probability is often approximated by the Henyey-Greenstein phase function:

$$p(\cos\theta) = \frac{1}{4\pi}\frac{1-g^2}{(1+g^2-2g\cos\theta)^{3/2}}$$

(3.1)

where g is the anisotropy factor, also known as the g-factor. It is defined as the average cosine of the angle between the incident light and the scattered light. The g-factor is defined in the range $-1<g<1$ where -1 corresponds to total backscattering and 1 corresponds to total forward scattering while for g equals zero we have isotropic scattering.
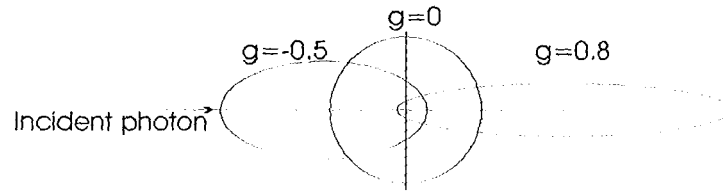

Figure 3.2 Description of the Henyey-Greenstein phase function for different values of the g-factor.

3.3.3 Transport equation

As stated before, the transport theory looks at the conservation of energy in an infinitesimal volume element in the media. This theory is described by the transport equation. This equation describes the change of the photon distribution function $N(\mathbf{r},\mathbf{s},t)$ $[\text{m}^{-3}\,\text{sr}^{-1}]$, by taking into account the change due to the incoming, outgoing and absorbed photons over this volume element.
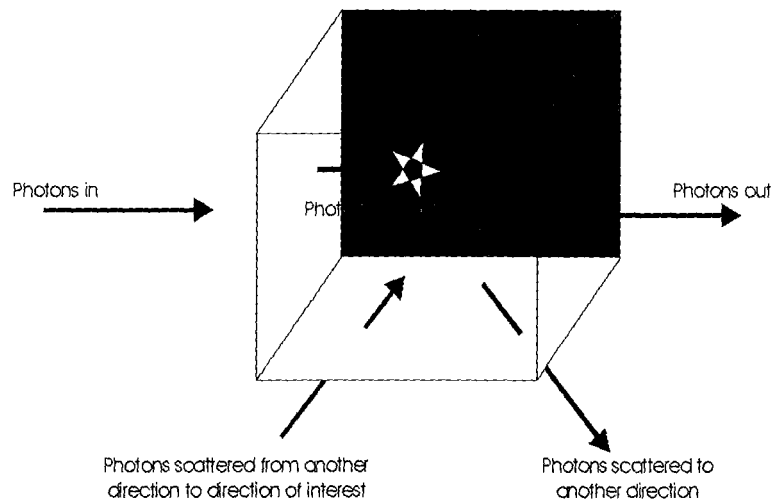

Figure 3.3 The transport equation is derived by considering the change of the photon distribution function over a small volume element.

By photon distribution function $N(\mathbf{r},\mathbf{s},t)$ we mean the number of photons within a small volume element around $\mathbf{r}$, which has a certain direction of propagation $\mathbf{s}$ at the time t.

Another property we need to use is the radiance $L(r,s,t)$ [W m^{-2} sr^{-1}], which describes the propagation of photon power. The radiance is derived by multiplying $N(r,s,t)$ with the photon energy and the velocity of light. However, neither the photon distribution nor the radiance can be measured directly. This is because the absorbers in the detector don't care about the direction of the photons propagation. To get a measurable quantity we define the fluence rate $\phi(r)$ [W m^{-2}] as the radiant power incident on a small sphere divided by the cross section area of that sphere. This is the same as integrating the radiance over all directions in space.

The most general transport equation is time dependent. However, this can easily be derived to the simpler time-independent transport equation, which is valid for the steady-state situation.

$$s \cdot \nabla L(r,s) = -\mu_s L(r,s) - \mu_a L(r,s) + \mu_s \iint_{4\pi} L(r,s')p(s,s')\,d\omega' + Q(r,s)$$

(3.2)

The term on the left-hand side of the time-independent transport equation describes the change of radiance in the direction of s. The first two terms on the right-hand side represent a loss of radiance in the s-direction. The first one is the amount of light being scattered away from s-direction whereas the second is the amount of light, propagating in s-direction, being absorbed. The third term is a gain term, describing the amount of photons originally travelling in any arbitrary direction that will be scattered into the direction s. The fourth term is another gain term representing a source in the volume element *e.g.* fluorescence or an optical fibre.

Although the transport equation is quite easy to derive and understand it is not an easy task to solve the equation analytically for a real problem. In order to be able to solve it we have to simplify the problem. We are going to study two methods in which this can be done, diffusion approximation and Monte Carlo simulations.

3.3.4 Diffusion approximation

The basic idea behind the diffusion approximation is to expand the transport equation into spherical harmonics. For the radiance this becomes

$$L(r,s) = \sum_{l=0}^{\infty} \sum_{m=-l}^{l} \sqrt{\frac{2l+1}{4\pi}} L(r)Y_{lm}(s)$$

(3.3)

If we only use the expansion in the first order of the expansion, we get

$$L(r,s) = A(r) + B(r) \cdot s$$

(3.4)

where A is the isotropic distribution and B is the linear gradient of the photon distribution function and s is the vector of the gradient. We insert this into the transport equation and simplify it.

$$-D\nabla^2 \phi(r) = -\mu_a \phi(r) + S(r)$$

(3.5)

This is the time-independent diffusion equation for an infinite homogenous medium where D is the diffusion coefficient:

$$D = \frac{1}{3(\mu_a + \mu_s(1-g))}$$

(3.6)

For the diffusion approximation to be valid, the light has to be diffuse. One requirement for this to be fulfilled is that the reduced scattering coefficient should be much greater than the absorption coefficient, $(1-g)\mu_s \gg \mu_a$. Another requirement is to avoid the region close to the source, whereas the photons in this region haven't had time to scatter and become diffuse yet. Moreover, when you use the diffusion equation to model the light distribution of a real case you have to consider boundary condition, geometry of your sample etc.

3.3.5 Monte Carlo simulations

A very efficient way to describe photon propagation in tissue is Monte Carlo simulation [9,10]. It is a stochastic model, which describes photons propagating through the media as a random walk. A photon or rather a photon packet is traced through the media until it exits at a boundary or is absorbed in the media. During the propagation process, it is possible to log different physical parameters of interest e.g. absorption position, time-of-flight, etc. If we repeat the propagation process for several photon packets, we'll be able to get a statistical distribution of the logged parameters, from which we then can calculate different physical quantities, as transmittance, absorption, fluence, etc.

For the simulation of a photon packet through the media, the Monte Carlo method begins by launching a photon into the tissue. In the beginning, the photon packet is assigned a weight W, representing the energy of the packet. When the photon propagates through the media, it travels for a distance s determined by

$$s = \frac{-\ln(1-\zeta)}{\mu_t}$$

(3.7)

before it interacts. In the equation above, ζ is a random number between 0 and 1 and μ_t is the attenuation coefficient, $\mu_t = \mu_s + \mu_a$. At the calculated interaction point, we need to determine if the photon is still in the media or if it has passed a boundary out of our system. If it has passed a boundary, a part of the photon packet is internally reflected while the other part is lost. However, in the event the photon is still in the media a part of the packets weight is absorbed in the media while the other part is scattered into a new direction. The amount of the weight being absorbed is

$$\Delta W = \frac{\mu_a}{\mu_t}$$

(3.8)

If the weight drops below a certain threshold value, it has limited impact on the logged parameters and a technique to terminate it is developed. If the packet is terminated is determined by a roulette technique, e.g. one chance in ten that the packet will survive. For the scattered part of the photon packet, the deflection angle is calculated using the Henyey-Greenstein phase function (3.1) using a new randomised number for the $\cos(\theta)$-factor. Since we have a uniformly distributed azimuthal scattering angle, we only need another randomised number to calculate it. Unless the photon packet is terminated or it has left the media, the process will start from the top by determining the stepsize s and going through these simulation steps again.

13

3.4 Single vs. multiple scattering

In this study, we are primarily interested in measurements on very thin samples. When using a thin sample the lights path right through the sample is very short. If it is a highly scattering media this is usually not a problem because the optical path through the media will be much longer and the photon will have scattered enough times to be treated as multiple scattered photon. However, if we have a thin sample and a dilute media, only one or a few scattering events will take place. This means that we can't treat the light as if it is diffuse and we can thereby rule out the diffusion equation as a way to solve the inverse problem. We now set our hope to that we'll be able to simulate the profile by Monte Carlo simulations. However, Monte Carlo doesn't take the single scattering properties phase and polarisation into consideration [8]. The question is therefore will we despite of this still be able to get correct results or will the loss of phase and polarisation create anomalies in the theoretical predictions?

Monte Carlo simulations uses the scattering- and absorption coefficient as well as the g-factor as parameters, but these parameters are defined in a macroscopic sense. Will they still be valid when studying the interactions microscopically? The g-factor uses the Henyey-Greenstein phase function to describe the angular scattering distribution but in the single scattering case, this is usually not a sufficiently accurate description. Moreover, the scattering- and absorption coefficients we use in the transport theory, are given by multiplying the scattering- and absorption cross section, given by the single scattering theory, with a factor proportional to the concentration of scatterers. However, this is only true for low concentrations of scatterers. If the concentration of scatterers is sufficiently high, the particles will be so close to each other that they influence each others near-field. This means that you have to consider the field from all the scatterers that are located close to each other to determine the behaviour of the scattering. In that case, there are no simple relations between the properties of the microscopic single scattering event and the properties of the transport theory [8].

As you can see in the discussion above there are some issues to consider when you are performing a measurement in this intermediate region, were you only have a single or a few scattering events. In literature, there is very little written about this intermediate region of scattering. Researchers are choosing to either work with single- or multiple-scattering, depending on what they are interested in studying. Researchers such as *van de Hulst*, who find that their sample is in the intermediate scattering region, often dilute it so they only have to consider independent single scattering [6]. This is a common approach when studying biological macromolecules, proteins etc. *Van de Hulst* also suggests a method to determine if you are in the single scattering region or not *"The intensity of a beam passing through the sample is reduced by extinction to exp(-t) of its original value. Here t is the optical depth of the sample along this line. If t<0.1 singel scattering prevails; for 0.1<t<0.3 a correction for double scattering may be necessary. For still larger values of the optical depth the full complexities of multiple scattering become a factor."* Only a few people work in the region where the have to take into account effects due to both single- and multiple- scattering. Consequently, there is no complete theory that describes the behaviour of scattering in this intermediate region. Therefore, we decided to increase the concentration of scatterers in our samples to avoid these problems.

3.5 Spatial resolved measurement techniques

Spatial resolved techniques uses the fact that the quantity of diffusely scattered light will vary as a function of the radial distance from the incident beam. Such a measurement will yield a profile of the diffuse scattered light, intensity vs. radial distance. The shape of this profile will vary depending on the optical properties of the tissue, so by studying the profile we can derive the absorption and scattering coefficients. If we look at the distribution of diffusely scattered light in a bulk media as in Figure 3.4,
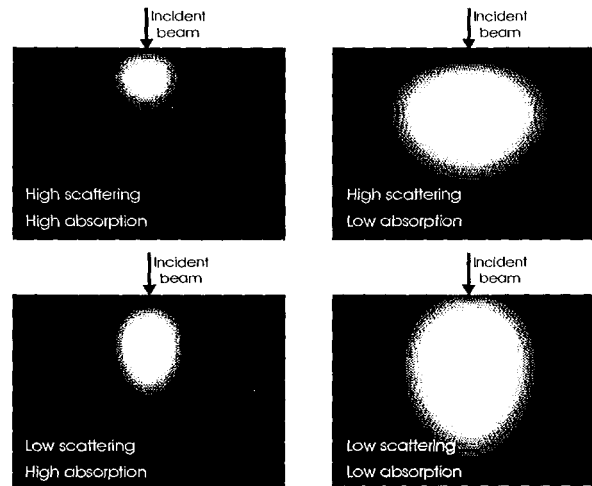

Figure 3.4 Cross section of the light distribution in bulk media depending on optical properties using the diffusion approximation, which behaves as if the source where located 1/μ'$_s$ into the medium.

it is easy to se how the profile will change due to the varying optical properties. With this technique, you can choose to study either the diffuse reflectance profile or the diffuse transmittance profile, depending on what you are measuring on and the design of your set-up.

To get a diffuse scattering profile you need to have some equipment that is able to make measurements at several different distances from the source [4]. We also desire that effects due to local property variations in our media should be minimised. This can be done by measuring the diffuse scattering at the same radial distance but in another or many direction from the source.

When we have acquired a profile, we need a method to derive the optical properties, to solve the inverse problem. One way to do this is to model the diffuse scattering with the diffusion equation (3.5), and then make a fit by using the optical properties as free parameters. The disadvantage of this method is that you are limited by that the diffusion approximation need diffuse light to be valid. In other cases, we can use the more general Monte Carlo simulation, and simulate the scattering profile for any optical properties of our choice. By doing that for a number of different optical properties we can create a set of profiles where each profile corresponds to a certain combination of μ_s, μ_a and g. Such a set is called a calibration set and by using that as a template, we can extract the optical properties from a measured profile with either a neural-network or multivariate analysis technique.

3.6 Data analysis

We have been using a multivariate analysis method to extract the optical properties from our measurements [11,12]. We will here briefly discuss some of the multivariate analysis techniques used.

3.6.1 Principal component analysis

Principal component analysis (PCA) is a way to reduce the number of variables we have to consider when doing multivariate analysis. How it works is perhaps best described by the three-dimensional case. Imagine that you have a distribution of data where the data points form a line through the three-dimensional space. After a principal component analysis, this system would be transformed to a one-dimensional system where all the data points lie along the axis, usually called the first principal component (PC1).
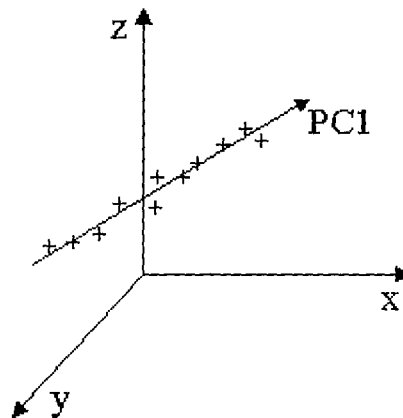

Figure 3.5 The first principal component (PC1) in the three-dimensional data space.

In the more complex case, you get the first principal component by positioning the axis along the direction of maximum variance, the second PC by positioning the axis orthogonal to PC1 and in the direction of the second largest variance, etc..

Therefore, instead of describing the scattering profile with a large number of different variables, where each represents the intensity at a certain radial distance from the incident beam, we can reduce this to 3 to 6 principal components and still describe the same scattering profile [2]. This procedure will make it easier to extract the optical properties with multivariate calibration.

3.6.2 Multivariate calibration

The first step of multivariate calibration is to create a model that describes the relation between some independent variables X, to some variables Y, that are dependent of the values of the independent variables. In our case, we want to relate how the variables describing the intensity at a certain radial distance from the incident beam, X, connects to the scattering- and absorption coefficients, Y. First, we have to train our model to know which optical properties a certain transmittance profile corresponds to. This is done by creating a calibration set consisting of both the transmittance profile and the optical properties that were used to simulate that profile. In a way, you can say that we teach the model by giving it the answers as well as the questions.

16

$$X_{Trans.\ profile} + Y_{Optical\ proproperties} \Rightarrow [Model]$$

When a model is created, we can us that to predict the dependent variables by just knowing the independent variables.

$$X_{Trans.\ profile} + [Model] \Rightarrow \hat{Y}_{Predicted\ opt.\ proproperties}$$

To get a more efficient calibration and prediction we usually reduce the number of variables in the problem by performing a principal component analysis beforehand.

4. Instrumentation

4.1 Introduction

As this equipment is research equipment that will be used to evaluate the technique for spatially resolved diffuse scattering in different measurement regions, the hardware is chosen so that it is flexible and adaptable. A zoom lens makes it easy to study diffuse scattering profiles of varying size. Using a zoom lens is also advantageous because of its non-contact quality. To increase the signal-to-noise ratio and to enhance the dynamic range of the detector, a silicon based photo detector is used instead of a CCD-chip. However, this introduces some new problems in alignment, zooming and focusing.

4.2 System set-up

The system can be used for either spatially resolved diffuse reflectance or spatially resolved diffuse transmittance measurements depending on the system set-up. This thesis is mostly dealing in the case of transmittance but for a test measurement, the system was rearranged for reflectance measurements.
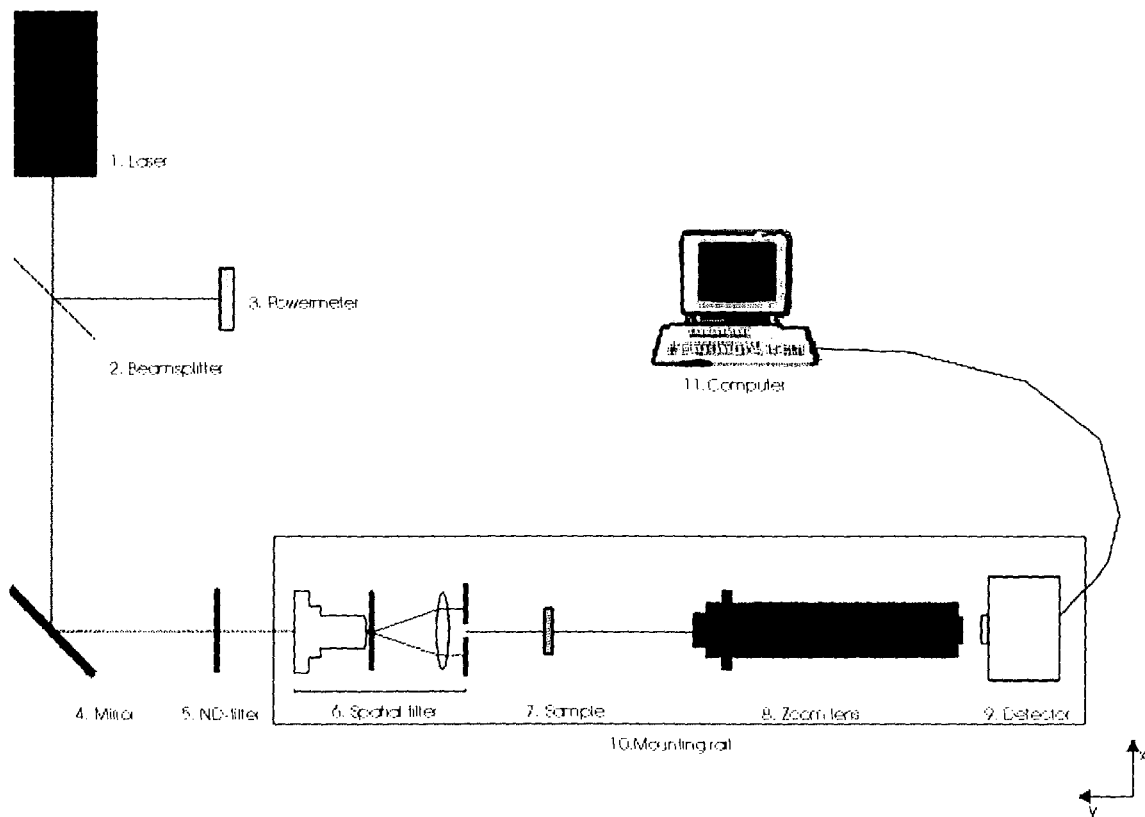
4.2.1 Transmittance

Figure 4.1 Schematics of the set-up for transmittance measurement (see also Appendix A, Figure A.1).

19

4.2.2 Reflectance

To reduce distortion due to the cuvette glass we mounted the detector and the lens vertically. This way we were looking at the surface of out scattering solution directly and avoiding an unnecessary glass plate inbetween the scattering surface and the detector.
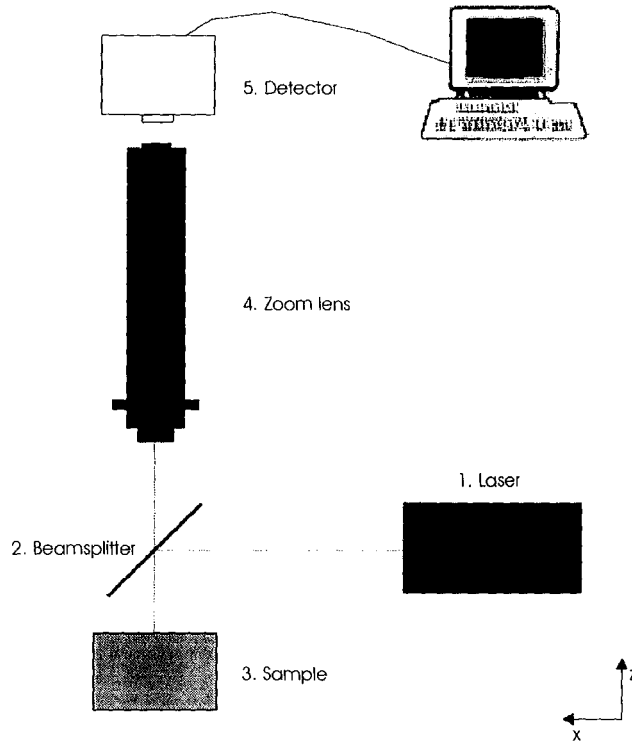

Figure 4.2 Schematics of the set-up for reflectance measurements.

4.3 Hardware description

4.3.1 Laser

The system is constructed to be able to use all visible light lasers with a wavelength within the detectors sensitivity range. We use a Siemens HeNe-laser, which emits at a wavelength of 632.8 nm. The laser has a maximum power output of 40 mW and a Gaussian beam with a diameter of 2 mm. (Figure 4.1: no. 1)

4.3.2 Powermeter

We want a reference signal to see if the laser output power is drifting. To get this we redirect a part of the beam with a beamsplitter and measure the power with a PHIR NOVA powermeter. (Figure 4.1: no. 3)

4.3.3 Spatial filter

To further collimate the beam we use a spatial filter, consisting of a 40/0,65-microscope objective and a 50 μm pinhole aperture and a f/60-recollimating lens. The lenses works

as a beam expander while the pinhole, put in the focal point of the lenses only let collimated light pass through. The spatial filter widens the beam diameter so to get the wanted beam size we use a 1-mm diameter aperture. (Figure 4.1: no. 6)

4.3.4 Zoom probe

The zoom probe consists of a detector and a zoom lens.

4.3.4.1 Detector

The detector is a so-called ring detector from AME in Norway (AE-9430). It has 16 concentric silicon photodiode rings approximately 0.28 mm wide with a spacing so that there are 0.3125 mm between the outer radius of neighbouring rings.

Figure 4.3 Ringdetector
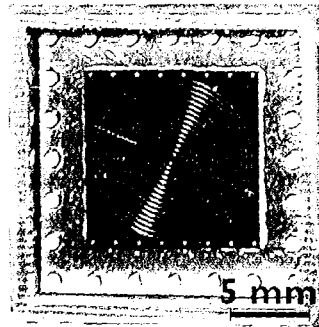
The detector is mounted on a printed circuit board and put in a metal housing. The circuit board is designed so that the signal from each detector ring goes through separate preamplifiers and each ring is connected to an individual channel on the data acquisition card [13]. (Figure 4.1: no. 9)
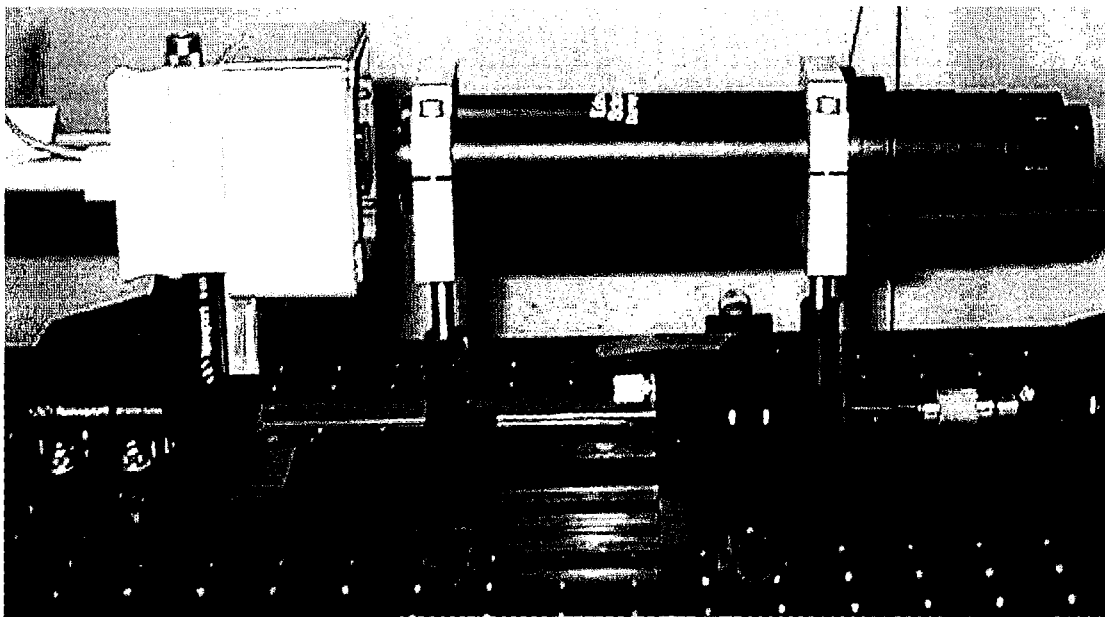
4.3.4.2 Zoom lens

Figure 4.4 Detector and zoom lens mounted on the mounting rail.

We use a parfocal zoom lens (Edmund Scientific, VZM model 450), with a magnification of 0.7X-4.5X. The parfocal zoom allows us to change magnification without having to refocus. The zoom lens is mounted in two separate lens holders, which makes it easy to align with Spindler & Hoyer microbench components. (Figure 4.1: no. 8)

4.3.5 Cuvette

When you are measuring on human or other biological media, it is advantageous and sometimes demanded that you only use a small sample. This is mainly because you don't want to draw to much blood or tissue from the patients. In addition, you often need a chemical, e.g. antigen, to react with the sample and create aggregates that will dominate the scattering. This chemical is rather expensive and for economical efficiency reasons the laboratory want to reduce the cost for the measurements. When you only have a small sample, you have to design the cuvette accordingly. It is also important that the geometry of the cuvette is well known so that the geometry specifications can be entered into the Monte Carlo simulations.

Two glass plates, 0.54mm thick, are fixated on both sides of a plastic plate, which have a keyhole shaped hole in it. The cuvette has an opening from the top of the cuvette.

We want to make sure that the distance between the two glass plates is the same as the thickness of the plastic plate (0.40-mm). To do this we press the two glass plates together on each side of the plastic plate with clips. The total thickness of the cuvette is 1.50 mm and the space between the two glass plates, the sample depth, will then become 0.42 mm.
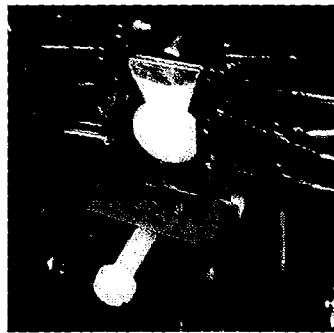

Figure 4.5 Cuvette filled with latex solution.

The reason for that the sample depth is greater than the thickness of the plastic plate is due to that the force applied by the clips to press the glass plates together are not high enough to press out the fluid that have come in between the glass plates and the plastic plate. However, the force is sufficient to hold the sample contained for the couple of minutes it takes to perform a measurement. To have the sample in the cuvette a longer time is not desired due to sedimentation in the cuvette that will affect the measurement.

A holder is created so that the cuvette can be mounted with microbench components. It is made of a small piece of aluminium that have a 4 mm wide slit with a depth of 5 mm and a plastic screw to fixate the cuvette. The holder is mounted on a xyz-stage, which makes it easy to centre the cuvette and put it in the focal plane of the zoom lens. (Figure 4.1: no. 7)

4.3.6 Mounting rail

The spatial filter, the cuvette, the zoom lens and the detector are all mounted on a mounting rail. This makes it easy to adjust the distances between the different components without too much disturbance and it also makes it easier to align the whole set-up. (Figure 4.1: no. 10)

4.4 Software description
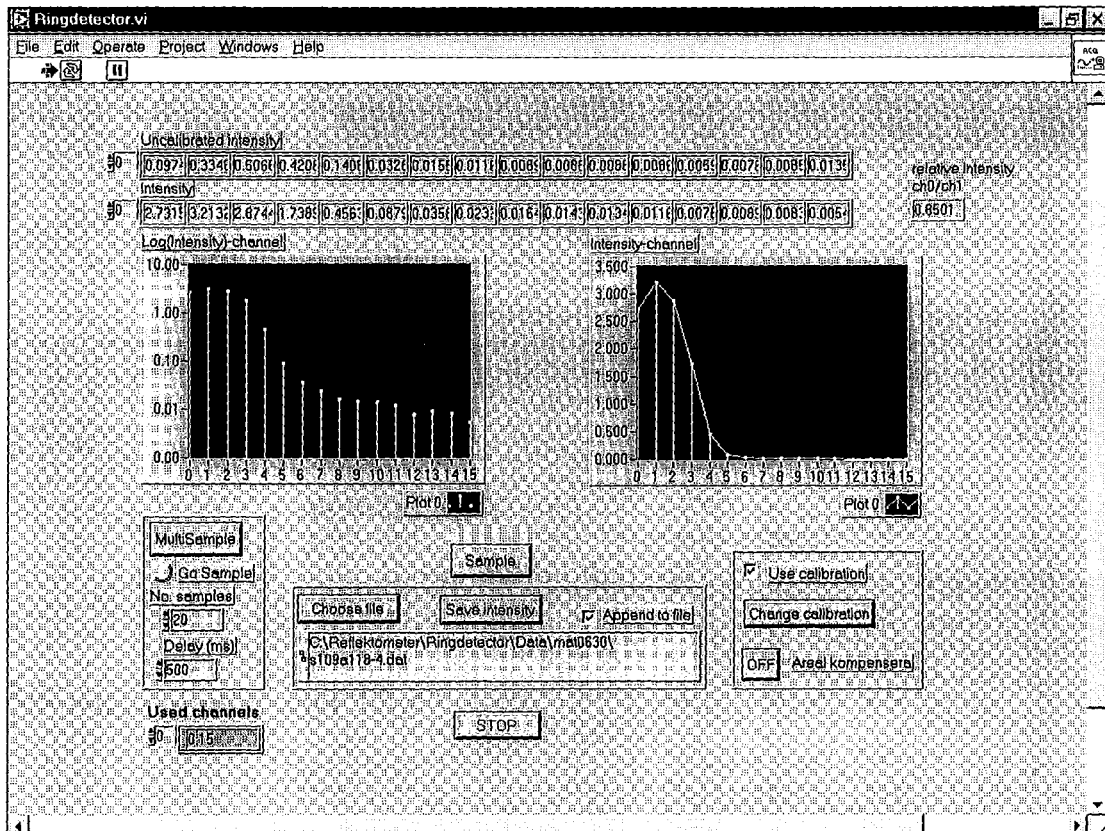
Figure 4.6 Main window of the data acquisition program.

The software is implemented in LabVIEW. The program works as follows: The data acquisition is started by pressing the sample button. The amount of acquisitions can be set as well as how fast this is done, default is to acquire 1000 readouts from the detector with a scan rate of 1000 scans per second. These signal data are averaged and the averaged signal data and their logarithm are plotted vs. their corresponding detector ring number. If desired the signal can be divided by the active area of the detector ring or divided by a special calibration vector (see section 4.5.4 Signal calibration). The data are thereafter saved into a file.

23

4.5 Set-up techniques

4.5.1 Alignment

One problem with this kind of detector is the need for perfect alignment. This is achieved in the following steps where the references are to Figure 4.1

1. Make sure that the laser (1) is parallel with the surface of the table.

2. Align the rail (10) so that the mounting positions are parallel with the laser beam. This is easiest done by mounting two apertures on the same height on each end of the rail and then move the rail until the light comes through the centre of both apertures.

3. Mount a spatial filter (6) in front of the first aperture and make sure the light hits the middle of the spatial filter and then still is going through the centre of the two apertures.

4. Mount the zoom lens (8) in the middle of the rail in between the two apertures and make the centre of the light go through both the apertures, unaffected of which zoom factor the zoom lens are set on. To fine adjust the alignment of the lens, replace the last aperture with a CCD camera. Put an OH-film with concentric circles printed on it, on the CCD-camera monitor. If everything is aligned properly the image of the light beam will increase in size concentrically and match the rings on the monitor while changing the zoom factor. If not correctly aligned, the centre of the beam will move while zooming. To make the zoom lens alignment easier, we put a x-stage under the front mount of the zoom lens.

5. When everything up to the zoom lens have been aligned, we remove the CCD-camera and replaces it with our detector (9) mounted on a xyz-stage and put the centre ring in the centre of the beam. To do this use a narrow beam, 1-mm in diameter and the 0.7x-zoom factor, and control that the beam hits the centre of the detector. To fine adjust, use the xyz-stage on which the detector is mounted and acquire data while moving the detector in xz-direction. Look at the ratio of the centrering/ring1, when you have maximised it you will have a well aligned system.

4.5.2 Zoom calibration

Figure 4.7 A printed circle with known diameter is used for zoom calibration.

We want to determine the zoom calibration, that is what magnification the current zoom setting correspond to, more exactly than what just reading the scale on the zoom lens (8) can give us. To do this we will change the sample (7) to a thin circle, 1-mm in diameter, printed on paper with a laser printer, see Figure 4.7. We widen the beam diameter to 2-mm, by changing the last aperture on the spatial filter (6) and centre the printed circle by adjusting the xyz-stage so that the circle casts a circular shadow on the ring detector (9). By doing this the signal from one or a few of the channels from the ring detector will be considerably reduced, see Figure 4.8. The zoom on the lens (8) is adjusted so that the shadow is hitting only one of the detector rings. We know the radius of the printed circle that we are imaging, we can see on what detector ring it is projected. By knowing the radius of the detector ring, we are able to calculate the zoom factor using the relationship in equation 4.1.

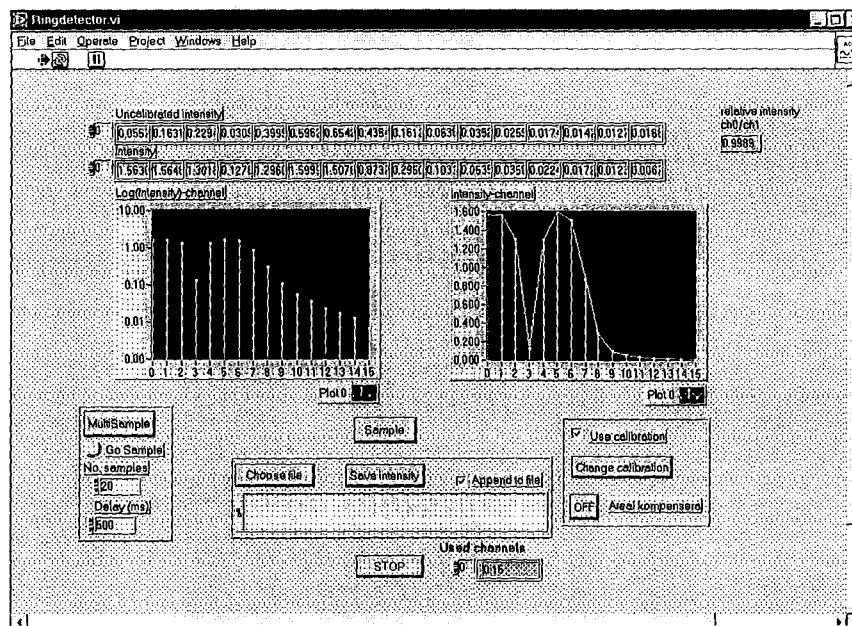$$\text{Zoom factor} = \frac{\text{radius of printed circle}}{\text{radius of detector ring}}$$

(4.1)

Figure 4.8 View of the main window when looking on the printed circle with known diameter.

25

4.5.3 Focus

The focus is set by knowing the focal distances of the zoom lens. The listed focal distance values of the lens are checked with a CCD-camera. The sample is set at the front focal plane 93 mm from the zoom lens front surface and the ring detector is put at the c-mount standard focal plane 17.5 mm from the lens back surface.

4.5.4 Signal calibration

The detector rings have different active areas. The further out from the centre, the greater area they have and consequently the higher signal will it give for a given illumination. To remove those effects as well as effects in the electronics we want to calibrate so that all detector rings register the same signal level when all the rings are illuminated with the same power. To do this the zoom probe is mounted on an optically integrating sphere into which the laser light is guided. The sphere will diffusely scatter the light and it will give an even illumination of the zoom probe looking into the sphere. Measurements of the intensity for each detector ring is taken and plotted as function of the detector ring area, Figure 4.9. An almost linear dependence is noticed, except for the signal from the outer ring that gives too high a signal. The reason for this has not been accounted for, but is believed to be caused by some unwanted reflection.
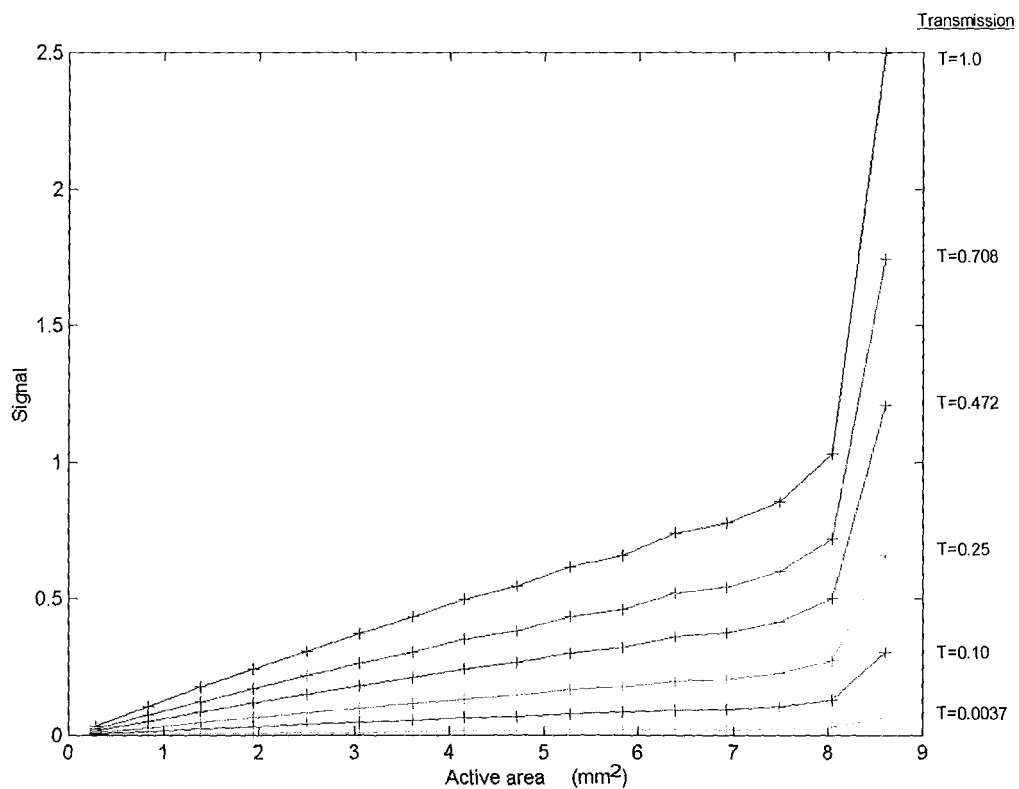
Figure 4.9 Signal vs. the active area of each detector ring for different relative transmission of light.

4.5.4.1 Power dynamic of detector

When performing signal calibration for each detector ring but with different NG (neutral grey) filters you will have similar curves but lower signal for higher damping. As seen by the Figure 4.10 the detector signals have a linear dependence of the transmission.

Figure 4.10 Signal vs. relative transmission for all detector rings.

5. Measurements & Simulations

5.1 Introduction

The measurements where done on different concentrations of solutions of 2μ-latex spheres to see that the theoretical model was applicable to the real measurements.

We choose the concentration of scatterers so that the scattering coefficient was in the region 437- 54 cm^{-1}. Doing so we got results that qualitatively corresponds to the theoretical predictions.
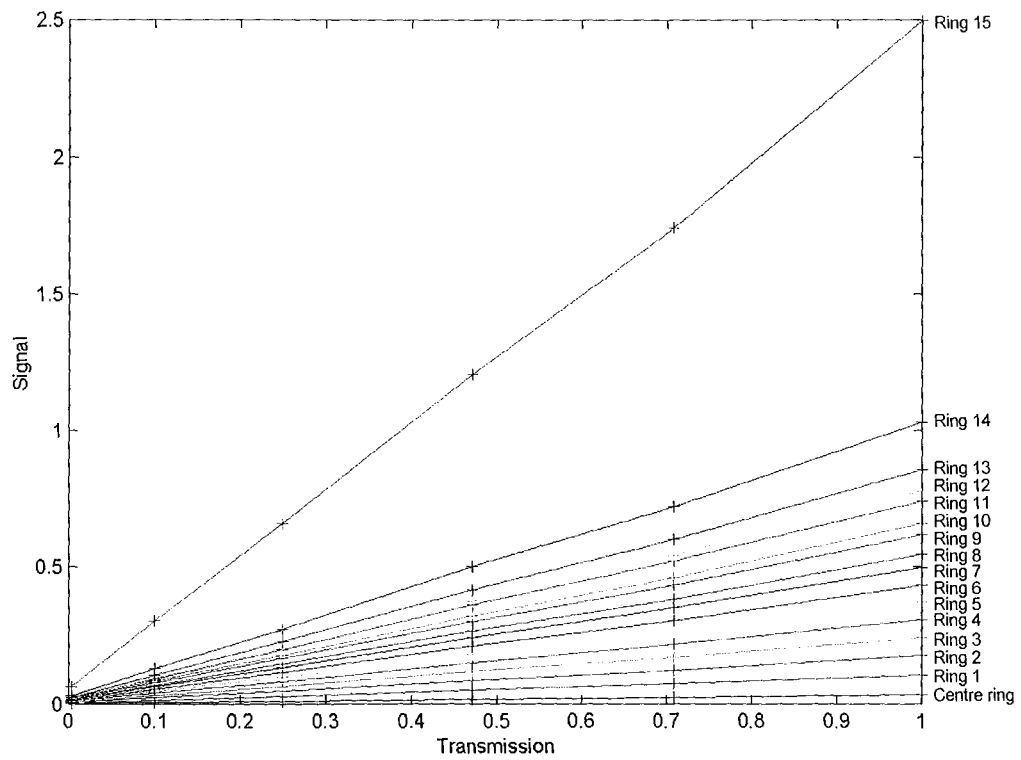
5.2 Method

5.2.1 Simulations

5.2.1.1 Geometry & optical properties.

When doing a Monte Carlo simulation, we design our model so that the input geometry parameters for the Monte Carlo simulations are consistent with the specified geometry of the cuvette. For each layer (see Figure 5.1), we specify the refractive index (n), the absorption coefficient (mua), the scattering coefficient (mus), the anisotropy factor (g) and the thickness of the layer (d). The layer structure of the cuvette will then be as in Table 5.1.

n	mua	mus	g	d (cm)	Description
1.00					Medium above (air).
1.52	0	0	1	0.054	Glass plate
1.33	μ_a	μ_s	0.917	0.042	Sample solution
1.52	0	0	1	0.054	Glass plate
1.00					Medium below (air).

Table 5.1 Layer structure of the cuvette as specified for the simulations, where μ_a and μ_s are free parameters that changes for different simulation runs.

We build one calibration set made up by of 60 simulations with varying absorption- and scattering coefficients covering the optical property ranges described by equation 5.1 and 5.2.

$$25 < \mu_s < 450 \ cm^{-1} \qquad (5.1)$$

$$0 < \mu_a < 2.0 \ cm^{-1} \qquad (5.2)$$

In addition to this, we also construct a prediction set, which will be used to validate accuracy of the data analysis. The prediction set consists of 10 simulations, where all the optical properties lie within the optical property space defined by the calibration set.

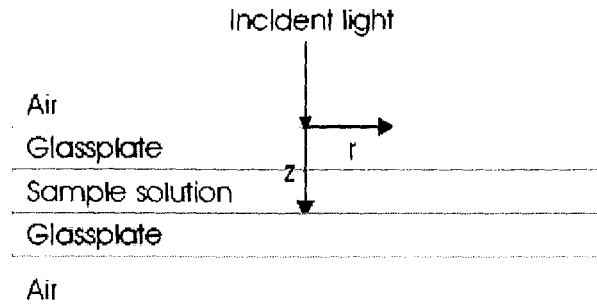### 5.2.1.2 Coordinate system and resolution.

Figure 5.1 A schematic of the layer structure and the coordinate system.

When simulating spatially resolved diffuse transmittance, the Monte Carlo program uses a cylindrical coordinate system [10]. The z-axis is oriented perpendicular to the surface of the cuvette, whereas r lies in the plane parallel to the surface of the cuvette and it denotes the radial distance from the incident light.

To be able to perform the simulation, we have to divide our model into a number of grid boxes. Each grid box represents a small volume element such as the one in Figure 3.3, over which we study the change in photon distribution. The smaller the grid boxes are the better resolution we will have in our results but we have to increase the number of photon packets to keep the same S/N-ratio. The simulation grid is chosen to have a resolution of 0.006 cm in the z-direction and a resolution of 0.01 cm in the r-direction. To accurately model the cuvette we use 25 grid boxes in z-direction and 40 grid boxes in r-direction, covering the entire depth of the cuvette and a radius of 4 mm.

We also have to choose the number of photon packets that we are going to simulate. The number of photons decides the precision and resolution we will have in our results. A simulation run with to few photons will produce a jagged transmittance profile, which we will be unable to compare with any measured profile whereas a simulation with a large number of photons will have a long execution time.

Because, we have a dilute media in a thin cuvette, which results in few scattering events, we decided to simulate 10,000,000 photon packets. This simulation took about 4 minutes for the fastest simulation and about 1 hour and 20 minutes for the most demanding simulation.

5.2.2 Beamsize

The Monte Carlo program performs its simulations with the approximation that we have an infinitesimally narrow incident beam. However, in any real measurement, it is impossible to produce an infinite beam, this difference in beamsize leads to poor results when we try to compare the measured and the simulated profiles. Fortunately, there is a method to transform the simulated infinite beam to a beam with finite size. This process is called convolution.

We want to decide the best diameter of the beam to be used both for our simulations and for our measurements. To do that we need to consider some factors related to our set-up and measurement and some factors due to the numerical calculations in our simulation and convolution.

One reason for the upper limit of the beamsize is due to the fact that we want to avoid any edge effects, like reflection in the cuvette sidewall. The upper limit of the beam diameter is therefore set so that the beam stays a certain distance from the cuvette sidewall at all times. Furthermore, when we are studying the diffuse transmittance profiles most of the information of the profile is in the region not directly illuminated by the beam. By studying some simulated profiles it seams reasonable to have the upper limit of the beam diameter set to ~6 mm. In addition, we don't want to use a too narrow beam since it would be more affected by inhomogeneities in the solution than a wide beam which illuminates more scatterers and averages over any inhomogeneities.

There are also numerical reasons for determining the beam diameter. When you convolute the infinite beam profile from the Monte Carlo program into a profile using a finite beam, you introduce an error due to the numerical calculations [10]. This error is caused by the fact that the Monte Carlo model only is defined in a finite space, given by the grid parameters (r, z) in the previous section. For the current grid parameters, beam diameters in the interval 0.6 mm to 3.5 mm are allowed.

To see if there was any difference between different beam diameters in this interval we convolute the simulations for three different beam diameters, 1 mm, 2 mm and 3 mm. The convoluted profiles were analysed with a multivariate calibration method to see if one of the beam diameters gave better predictions and less error. However, there were no big differences between the different runs.

Considering all of this a tophat beam with a diameter of 1 mm was chosen.

5.2.3 Measurements

5.2.3.1 Absorption

As absorber, we use a green food dye. We want to know how the absorption for a solution changes with increasing concentration of this dye. There are no tables where we can look this dependence up and even if there were, the absorption coefficient would probably differ between different shipments of the dye. Therefore, we need to do a series of measurements on solutions with different concentrations of the absorber.

The measurement will determine the absorption coefficient by using Beer-Lambert's law.

$$\frac{I_t}{I_i} = e^{-\alpha h}$$

(5.3)

Where I_t is the transmitted light, I_i is the incident light and h is the distance the light has travelled true a medium. The coefficient α is the extinction coefficient depending on the concentration of absorbers and scatterers in the medium.

We know the geometry of the cuvette and therefore the thickness of the sample. When we only have the dye dissolved in distilled water, multiple scattering will be negligible and the distance the light will travel through the medium will be equal to the thickness of the sample.

31

To get higher accuracy we start by diluting the dye 500 times and use this as our base in all our following measurements. We obtain seven different concentrations of the dye by diluting it 500, 1000, 3000, 4000, 5000, 6000, 15000 times. We calculate a concentration out of this by setting the pure food dye concentration to 1 and thereafter calculate the concentration when it is diluted 500 times and so on.

In the measurements, we used a PHIR Nova powermeter. We started by taking a reference of the incident light, I_i, by measuring on a cuvette filled only with distilled water. Thereafter we measured the transmitted light for the different concentration of absorber.

By plotting $\log(I_t/I_i)/h$ vs. the concentration of the sample as in Figure 5.2, we obtain a linear dependence of how the absorption coefficient depend on the concentration of the absorber. We made a linear fit and extract equation 5.4.

$$\mu_a = -0.4027 + 3173 \cdot \text{Concentration} \qquad (5.4)$$

We notice that there have to be something wrong with the absorption measurement, because the absorption coefficient can't be negative, as it would be for concentration equal to zero in eq. 5.4.
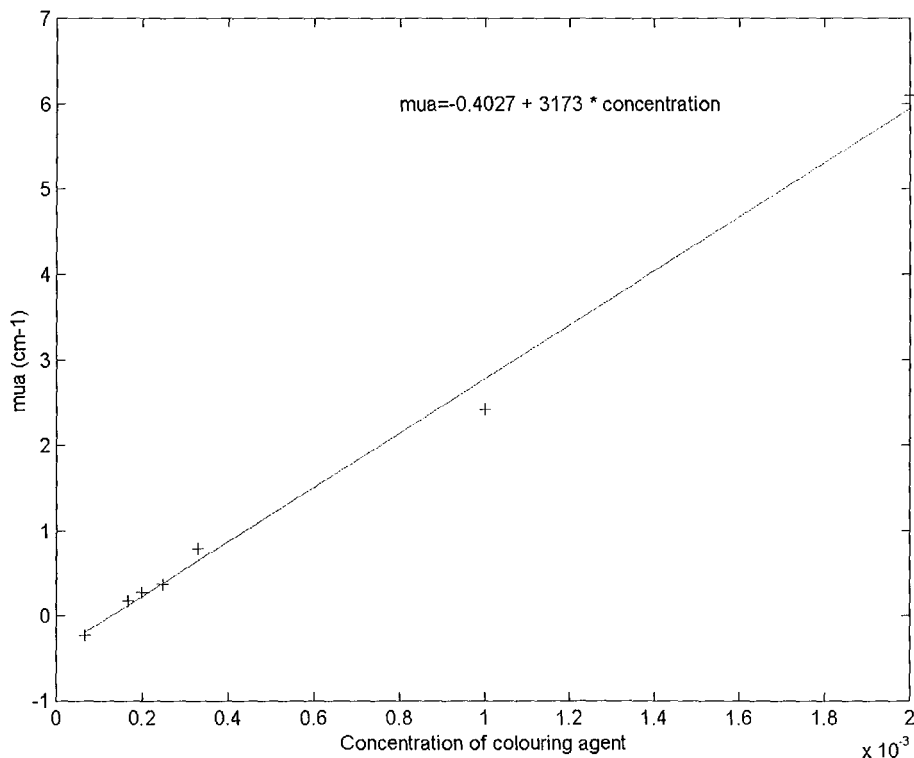

Figure 5.2 Plot of $\log(I_t/I_i)/h$ vs. the concentration of colouring agent with a linear fit made to the measured data.

32

5.2.3.2 Scattering

In our measurements, we will use latexspheres[*] with a diameter of 2 μm as scatterers.

5.2.3.2.1 Mie calculations

To know the scattering coefficient for different concentrations of scatterers we calculate it using a Mie scattering program[†]. The parameters entered into the Mie calculations are given by the technical specifications of the latexspheres, see Table 5.2.

Latex, refractive index	1.5866
Water, refractive index	1.333
Sphere diameter	2.00 μm
Latex, specific weight	1.050 g/ml
Water, specific weight	0.997 g/ml
Wavelength	630 nm

Table 5.2 Input parameters for the Mie calculation.

For the different concentrations of scatterers The Mie calculations yields the following results, see Table 5.3:

Conc	mus [1/cm]	g
0.00235	54.670252	0.916585
0.0047	109.340504	0.916585
0.0094	218.681009	0.916585
0.0188	437.362017	0.916585

Table 5.3 Results of the Mie calculation for different concentration of scatterers.

5.2.3.3 Mixing method

For the ease of combining different concentrations of scatterer with different concentrations of absorbers, both the scatterer and the absorber are mixed to the double concentration so that they can be combined by taking a equal part of both, see Table 5.4 and Table 5.5.

---

[*] Bangs Laboratories, Inc.

[†] "Sphere mie scattering program" written by Wang and Jacques.

5.2.3.3.1 Scatters

As the latexspheres we have bought are dissolved in distilled water, we have to start our mixing by diluting this original solution of 9.4 % latexspheres in water to the desired concentration. Before any diluting is started we let the bottle with the original solution lie in a sonic bath for 3 minutes, this will separate any lumps of latex spheres that may exist in the solution. To get the best accuracy we dilute our solution in a repetitive way. This means that we start mixing the solution with the highest concentration of scatterers and then using that one as a base for mixing the solution with half that concentration and so on.

μ_s for half of the concentration (cm^{-1})	Concentration
437	3.76 %
218	1.88 %
109	0.94 %
54	0.47 %

Table 5.4: Scattering mixing. Where concentration is the amount of scatterers there are disolved in distilled water .

5.2.3.3.2 Absorbers

μ_a for half of the concentration (cm^{-1})	Concentration
1.69	1.33 ‰
1.18	1.0 ‰
0.65	0.67 ‰
0	0.00 ‰

Table 5.5: Absorption mixing. Where concentration is the amount of pure colouring agent disolved in distilled water.

The scatterer and the absorber are mixed to give 10 different samples with the following combinations of optical properties:

Sample no.	1	2	3	4	5	6	7	8	9	10
μ_s (cm^{-1}):	54	109	109	109	109	218	437	437	437	437
μ_a (cm^{-1}):	0	0	0.65	1.18	1.69	0	0	0.65	1.18	1.69

Table 5.6 Ten samples with different combinations of optical properties.

5.2.3.4 Measuring method

To minimise any effects caused by the cuvette or having to do with how the cuvette is mounted in the set-up, we use four replicates consisting of two different cuvettes viewed from two different sides. The measurement series start of by taking a background measurement by putting a highly absorbing material in the cuvette holder. During this measurement and in all the forthcoming measurements we are taking a reference signal of the output intensity from the laser. This way we can divide our measured transmittance profile with the reference value to get values that are unaffected by the fluctuations of the intensity of the incoming beam. The measurements on our samples are done in the following way. We fill the cuvette as described in the next section. Then we put the cuvette in the cuvette holder and turn of any reading lights. We note the laser output signal and acquire data 10 times during a time span of 15-20 seconds. This is done to average out effects that vary over a short time interval, *e.g.* small fluctuations of the laser intensity or movements of any inhomogeneities in the cuvette. We save the data, pick up the cuvette, turn it half a turn, and put it back. Thereafter we acquire a new set of data and its corresponding reference signal. When this is done we start over with a new sample.

5.2.3.4.1 Cuvette filling

To fill the cuvette with the mixed solution we go through the following steps:

1. Hold one of the glass plates between your tumb and indexfinger.

2. Put the plastic plate, that will be used as a spacer, on the glass plate and center the opening in the plastic plate.

3. Put your test-tube with the scattering solution on a shaker an shake it for a while so that no latexspheres are settled on the bottom of the tube and no inhomogeneities are visible.

4. Use a pipette to take a small sample of the scattering solution and put a drop in the centre of the glass plate that you hold. It is important that there are enough solution filling the hole in the plastic plate more than well.

5. Apply the second glass plate on top, so that the solution is contained between the two glass plates.

6. Fixate the glass plate with two clips.

5.3 Results

5.3.1 Simulations

We test the accuracy and robustness of the data analysis in the desired region of optical properties. This is done by using the calibration set to teach our data analysis model which optical properties a certain scattering profile corresponds to, as described in section 3.6.2. We then try to predict the optical properties of our prediction set, which lie within the optical properties region of our calibration set, by just looking at the scattering profile. Thereafter we compare the predicted results with the known optical properties from our simulated prediction set and measure the correlation.
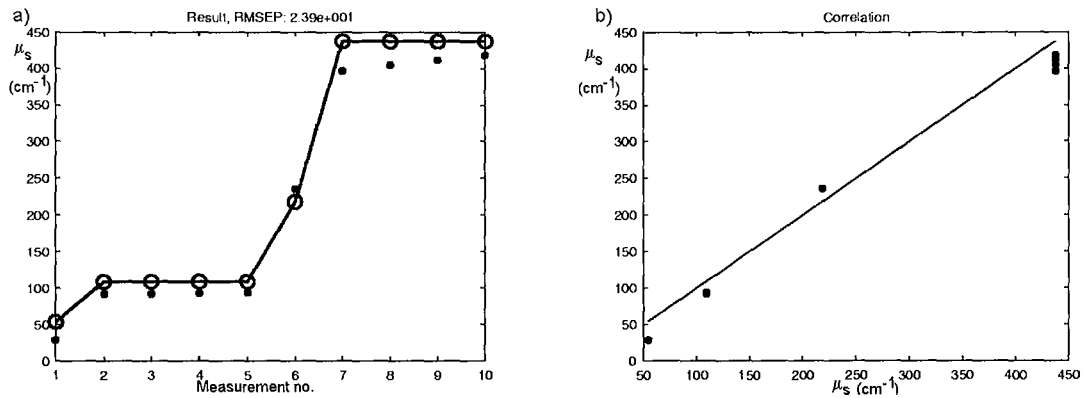

Figure 5.3 a) Predicted values (•) for the scattering coefficient compared to the known values (o) given by our simulations. b) The correlation between predicted (•) and known values of the scattering coefficient.

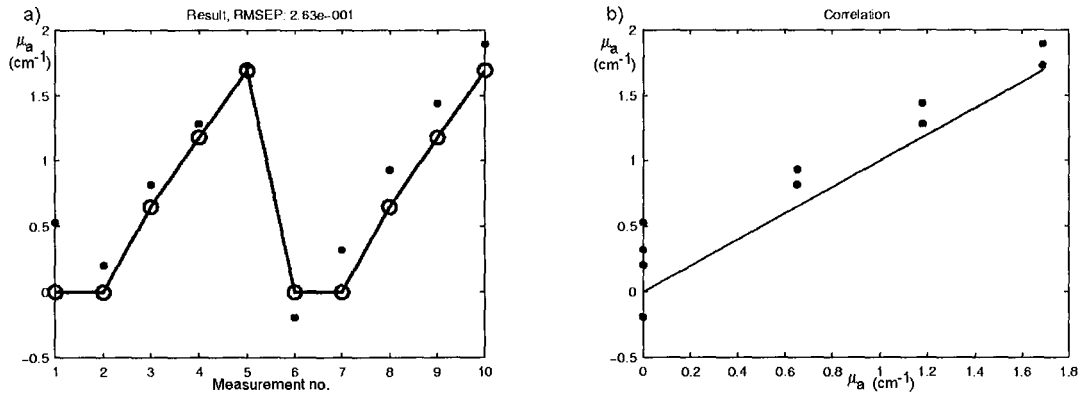Figure 5.4 Predicted values (•) for the absorption coefficient compared to the known values (o) given by our simulations. b) The correlation between predicted (•) and known values of the absorption coefficient.

We see that the predictions match the known values reasonably well. If the values didn't match it could depend on that we had chosen too large steps in the calibration set which makes it hard to predict the optical properties when we are interpolating between two different simulations of the calibration set. Alternatively, it could depend on that our simulation data is noisy, this means that we have a very jagged scattering profile. Noisy data could mean that there are differences in the scattering profile even between two simulations with the same optical properties. Naturally this makes prediction hard

or impossible depending on the degree of noise. The solution to this problem is to insert more photons into the simulation, which gives a smother and not as noisy scattering profile.

5.3.2 Measurements

5.3.2.1 Qualitatively

To see how well the theory fits the measurement we want to compare the Monte Carlo simulated transmittance profiles with the measured transmittance profile. In order to be able to compare the profiles we scale the measured transmittance profiles so that the profile with $\mu_s = 218$ cm^{-1} match its simulated equivalent. Figure 5.5 shows the simulated transmittance profiles for the same optical properties as our samples are mixed to correspond to.
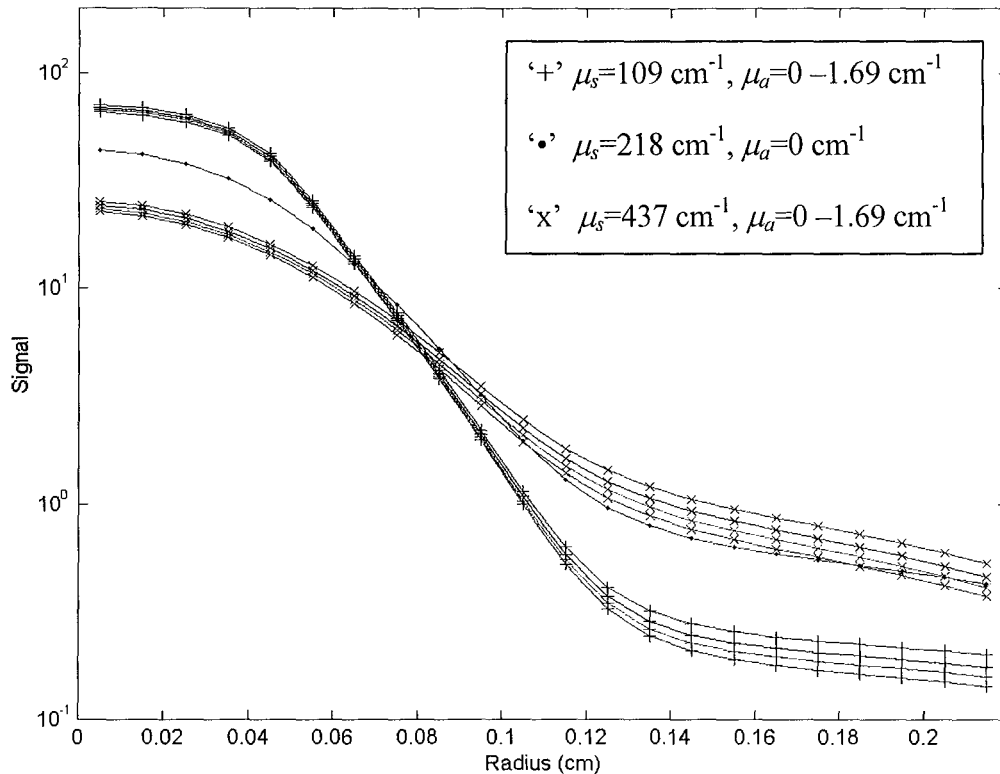

Figure 5.5 Simulated transmittance profiles.

Figure 5.6 shows the measured transmittance profiles for the samples that we mixed in section 5.2.3.3.3. When we did the measurements, we used four replicates for every sample but we have for display reasons only plotted the average profiles of these replicates. For each set of profiles with a certain scattering coefficient, the profile with the highest signal at far distance from the centre is the one with the lowest absorption coefficient.

To be able to compare the measured profiles with the simulated profiles absolute we overlay a selection of the measured profiles with the same selection of simulated profiles, see Figure 5.7.
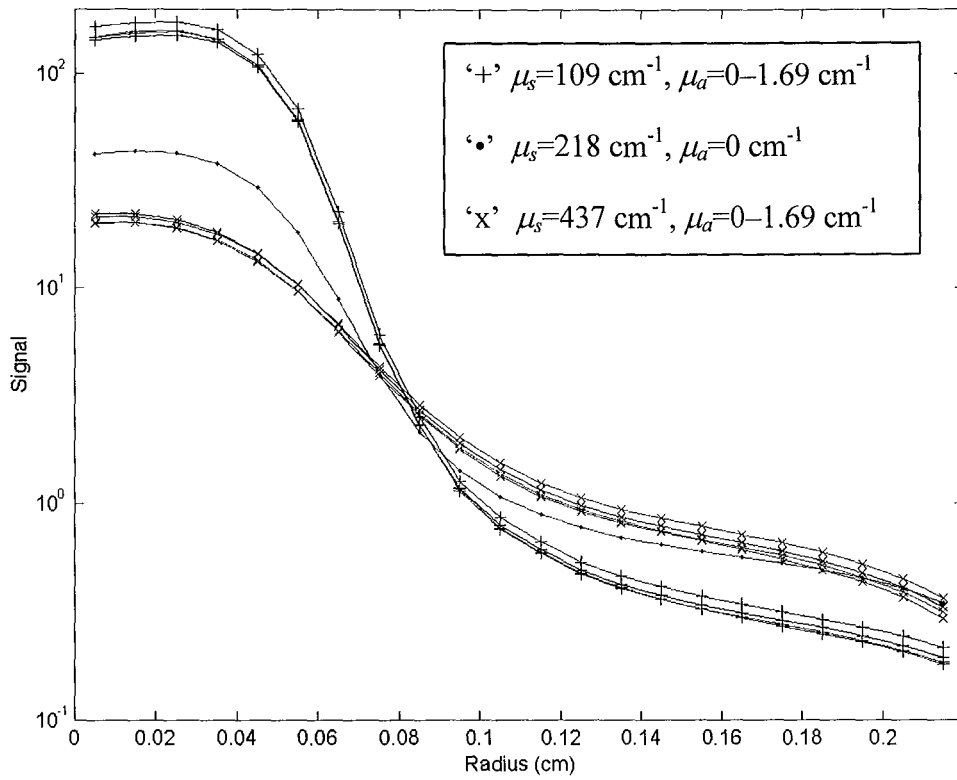
Figure 5.6 (graph)

y-axis: Signal
x-axis: Radius (cm)

Legend:
'+' μ_s=109 cm^{-1}, μ_a=0–1.69 cm^{-1}

'•' μ_s=218 cm^{-1}, μ_a=0 cm^{-1}

'x' μ_s=437 cm^{-1}, μ_a=0–1.69 cm^{-1}

Figure 5.6 Measured transmittance profiles.

Figure 5.7 (graph)

y-axis: Signal
x-axis: Radius (cm)

Legend:
'+' μ_s=109 cm^{-1}, μ_a=0.65 cm^{-1}

'•' μ_s=218 cm^{-1}, μ_a=0 cm^{-1}

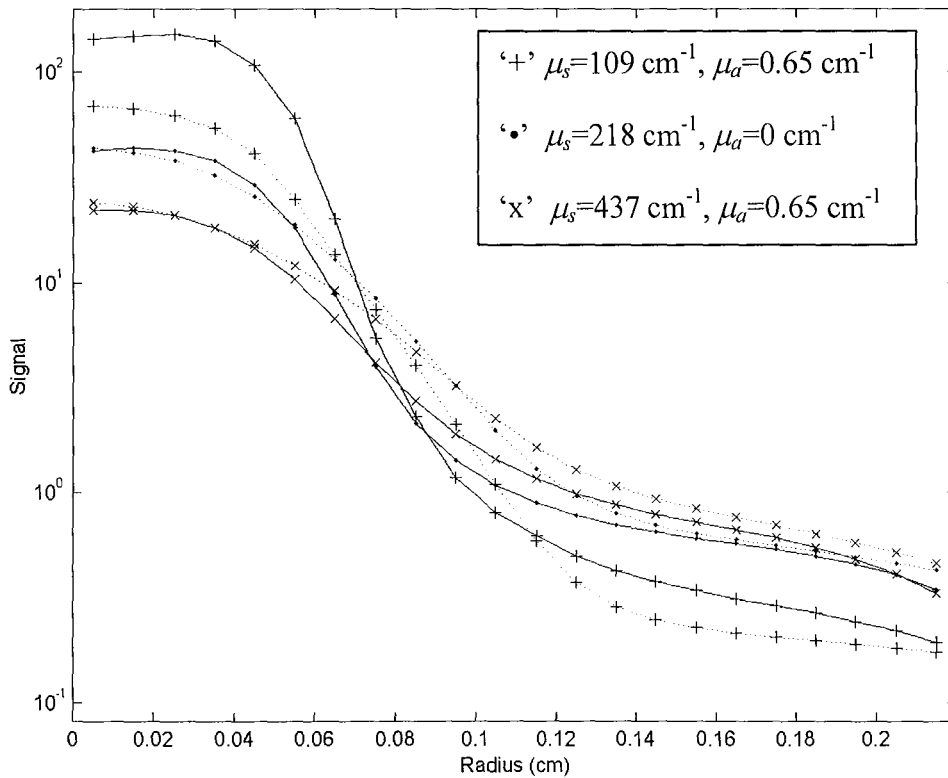'x' μ_s=437 cm^{-1}, μ_a=0.65 cm^{-1}

Figure 5.7 A comparison simulated (.) and measured (—) transmittance profiles for a selection of optical properties.

5.3.2.2 Data analysis

To evaluate our data even further we use the data analysis model to see how well it can predict the optical properties by looking at the transmittance profiles. First, a principal component analysis is performed. Normally you need at least one principal component per property you want to predict, which would mean two in our case. However, we got less prediction errors in the scattering when we reduced the 22 variables of each transmittance profile into three principal components. Thereafter we do a multivariate calibration.

As we could see in Figure 5.7 the measured and simulated profiles doesn't match completely. Nevertheless, we will still try to use the simulation profiles as calibration set, and then predict the optical properties by looking on the measurement profiles, see Figure 5.8 and Figure 5.9.
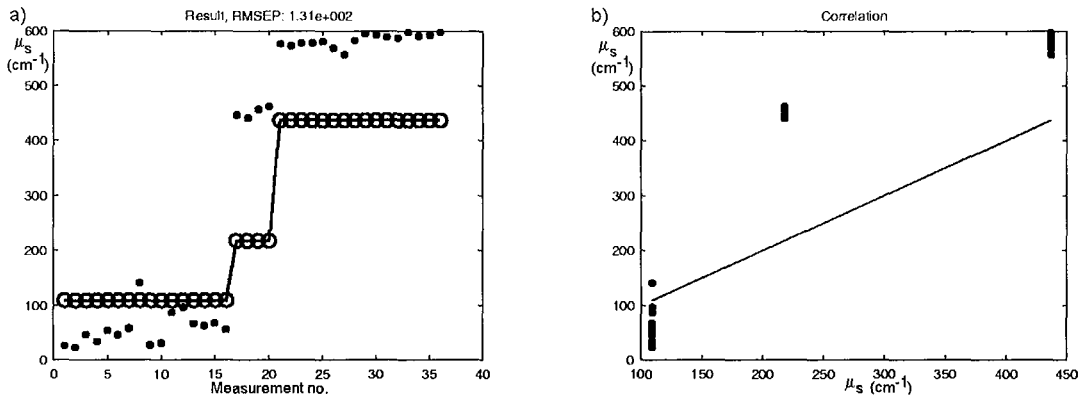

Figure 5.8 a) Predicted scattering coefficients (•) obtained by using the measured profile as prediction set compared to the values (o) given by the known concentration of scatterers. b) The correlation between predicted (•) and known values of the scattering coefficient.

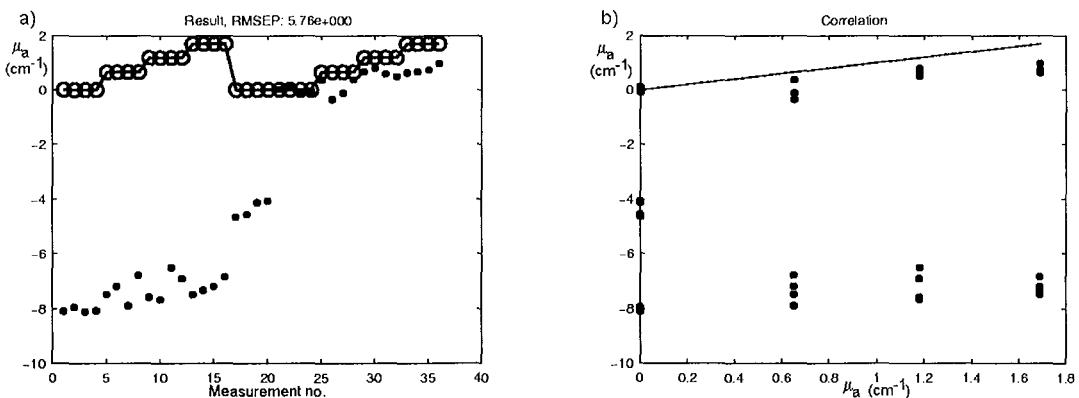*Figure 5.9 a) Predicted absorption coefficients (•) obtained by using the measured profile as prediction set compared to the known values (o) given by the known concentration of absorbers. b) The correlation between predicted (•) and known values of the absorption coefficient.*

39

As guessed in advance, these predicted optical properties correlate poorly with the optical properties that the samples are mixed to correspond to. So, instead of using the simulated profiles as calibration set, we use half of the measured profiles as calibration set. Thereafter we predict the optical properties of the other half of the measured profiles, see Figure 5.10 and Figure 5.11.
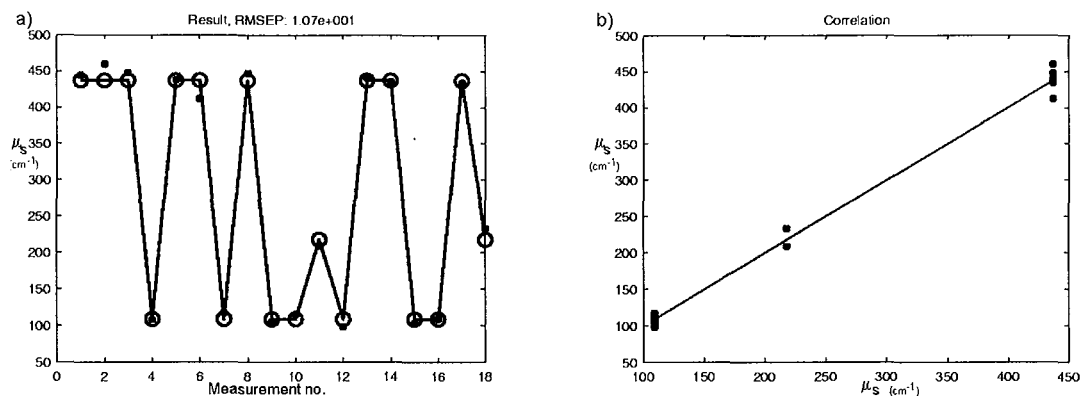

Figure 5.10 We use half of the measured profiles as prediction set and the other half of the measured profiles as calibration set. We then compare the known values (o), given by the known concentration of scatterers, to the predicted scattering coefficients (•) obtained by the measured transmittance profiles. b) The correlation between predicted (•) and known values of the scattering coefficient.
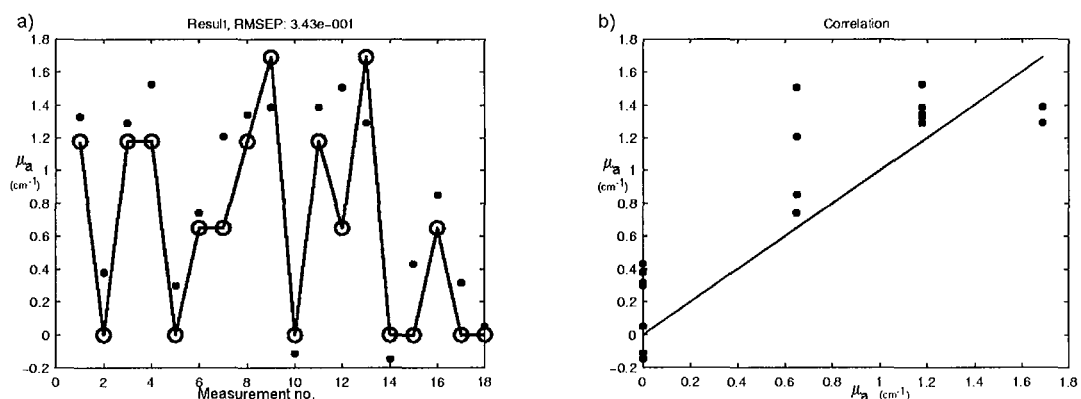

Figure 5.11 We use half of the measured profiles as prediction set and the other half of the measured profiles as calibration set. We then compare the known values (o), given by the known concentration of absorbers, to the predicted absorption coefficients (•) obtained by the measured transmittance profiles. b) The correlation between predicted (•) and known values of the absorption coefficient.

6. Discussion

6.1 Results

As seen in the previous chapter, the measurements did not correlate very well with the theory of the simulations. However, we can se a qualitative similarity between the measured profiles and the simulated profiles. Furthermore, if we normalise the transmittance profiles, by scaling the profiles independently of each other, we can see that the shape of the profiles match considerably better to their corresponding simulated profile shape than what the absolute signal levels do. The reason for this has not been completely established. However, one explanation could be a back reflection either from the gold plated ring detector (Figure 4.3) or from the lens itself. The reflection will illuminate the sample and increase the signal level of the measured transmittance profile. When we have the least number of scatterers, μ_s=109 cm^{-1}, we have the more light passing right through the cuvette compared to the samples with more scatterers. This also means that a sample with low scattering coefficient will reflect back more light to the cuvette than a sample with high scattering coefficient. Therefore, the samples with low scattering will have a greater increase of the signal level due to the back reflection than a sample with high scattering will have. This all agrees with how the measured profiles are displaced in regard to the simulated profiles. However reasonable this possible explanation is, it was thought of quite late in this project so no tests were made to try the verify it. One way around the problem that the signal levels of the transmittance profiles do not match, is to normalise the profiles. This is done by choosing one point at a certain radial distance where all the profiles have the same value. This point is often chosen to be where all the simulated profiles cross each other which in this case is around r=0.08 cm. Although in general, normalisation of the measurements leads to increased prediction errors compared to there absolute equivalent [2].

When trying to predict the absorption coefficient, as in Figure 5.9 and Figure 5.11, we obtain much larger prediction errors than when predicting the scattering coefficient. One reason for this could be that the variance is so much smaller in the absorption case than in the scattering case which makes it hard to predict when the measurements does not fit the simulations very well. Another reason is the third principal component that we use in the data analysis. If we would change the number of principal components to two we would get a better prediction of the absorption, but unfortunately we would get larger prediction errors of the scattering coefficient.

To use half of the measured profiles as a calibration set and predict the optical properties of the other half seem to give reasonably accurate predictions, see Figure 5.10 and Figure 5.11. However, to draw any conclusions of the data analysis and the measurements in our case wouldn't be completely valid. We have 10 different samples which each has 4 replicates, 40 measurements in all. When half of these measurements are randomly selected to be the calibration set and the other half is selected to be the prediction set, then it's hard not to get very similar profiles in both the calibration set and the prediction set. This will lead to better predictions than it would have been if the prediction data were separated more from the calibration data.

6.2 Instrumentation improvements

6.2.1 Cuvette

Different methods were tried out to make the cuvette. The most successful where to just press the two glass plates together on each side of the plastic plate with clips. A further improvement of the cuvette would be to make it easier to fill. This could be done by using capillary pressure to draw the sample fluid into the cuvette. This method was tried for this cuvette but the sample space where to big, and it didn't fill properly. If the current method of filling the cuvette is used, a circular hole is preferred instead of the keyhole shaped hole of the current design.

6.2.2 Focus

The method used in zoom calibration was tried to get an accurate focus. The idea behind this was that when a printed circle is centred so that it would shadow one ring, the ring would be blurred when the system is unfocused, giving a not as sharp shadow. The blurring would be noticed due to the fact that the neighbouring channels would get lower signal as well as the ring centred channel. However, this didn't work out as well as wanted, at near focus the signal changes were to small to give any guidance how to adjust the focus. This could possibly be improved by using a better-dimensioned printed circle with higher sharpness than what a 600-dpi laser printer can produce. This could for example be done in some lithographic process or by photographing bright rings and using the film negative. The simplest way could be to buy circular pattern comparator-reticles with well-defined size. One problem with that is that if the ring background is transparent there will hardly be any blurring of the ring.

7. Conclusions

This thesis has been dealing with the development of a zoom probe for spatial resolved diffuse transmittance studies. Due to the detector type, several technical problems where introduced into this project, problems that would have been avoided if a CCD-detector was used instead of a ring detector. Many of these problems were solved, such as zoom calibration, focusing, alignment. However, when we started the measurements, there were still some uncertainties about the system. The performance of the zoom probe was tested on solutions of latex spheres. The measurements show a qualitative correspondence to the theory whereas the absolute measurements do not match very well. The ring detector seems not to be the best choice of detector for measuring the optical properties, due to the technical problems. However, the goal of this project was not solely to measure the optical properties. Just as important were to evaluate the ring detector as a new, low cost method to measure these properties. As for designing a flexible research equipment I would advise against the use of the ring detector and instead replace it with high resolution CCD-camera. However, a CCD-camera with the same power dynamic range and the same high signal-to-noise ratio costs considerably more and also has the drawback that it need to be cooled. Consequently, if the final goal is to produce a low cost diagnostic instrument, the ring detector could still work well, as soon as the remaining problems with the set-up are solved.

8. References

1. L. Øgendal, "Lysspredning" (KVL 1995)

2. J. S. Dam, P. E. Andersen, T. Dalgaard, P. E. Fabricius, "Determination of tissue optical properties from diffuse reflectance profiles by multivariate calibration" Appl. Opt. Vol 37, No. 4, 1998.

3. I. M. Roitt, "Roitt's essential immunology" (Blackwell Science, Oxford 1997)

4. Optical Thermal Response of Laser Irradiated Tissue edited by A.J. Welch and M.J.C. van Gemert (Plenum Press, New York,1995)

5. C. F. Bohren and D. R. Huffman "Absorption and scattering of light by small particles" (John Wiley & Sons Inc., New York, 1983)

6. H. C van de Hulst, "Light scattering by small particles" (Wiley, New York,1957)

7. C. af Klinteberg, "On the use of light for the characterization and treatment of malignant tumours" (Lund Reports on Atomic Physics, 1999, LRAP-245)

8. A. M. K. Enejder, "Light scattering and absorption in tissue –models and measurements", (Lund Reports on Atomic Physics, 1997, LRAP-219)

9. S. A. Prahl, M. Keijzer, S. L. Jacques, A. J. Welch, "A Monte Carlo Model of Light Propagation in Tissue", (SPIE Institute Series Vol. IS 5 ,1989)

10. L. Wang and S. L. Jacques,"Monte Carlo modeling of light transport in multi-layered tissues in standard C", (Laser Biology Research Laboratory, M. D. Andersson Cancer Center, University of Texas, Houston, Tex. 1992)

11. R. Bro, "Håndbog i multivariabel kalibrering", (DSR tryk, 1996)

12. K. Esbensen et al., "Multivariate Analysis in practice", (CAMO ASA, Norway, 1998)

13. C. Pedersen, "Zoom probe hardware" (Internal B&O project document, 1999)

9. Acknowledgement

I would like to thank my supervisor Jan Sørensen Dam for all the support during this project. I would also like to thank Stefan Andersson-Engels for all the help with understanding the theory.

Thanks also to all the people at Bang & Olufsen Medicom for the very nice stay I had in Struer. I would especially want to thank Paul Erik Fabricius, Carsten Pedersen and Torben Dalgaard, for all the help with the hardware and the data analysis.

Special thanks to Hedda Malm for reading through the report and making me aware of some of the grammatical errors. However, any remaining language errors are completely my mistakes. Finally, I would like to thank all my friends who continued to listen when I got started to talk about what I was doing in this project.
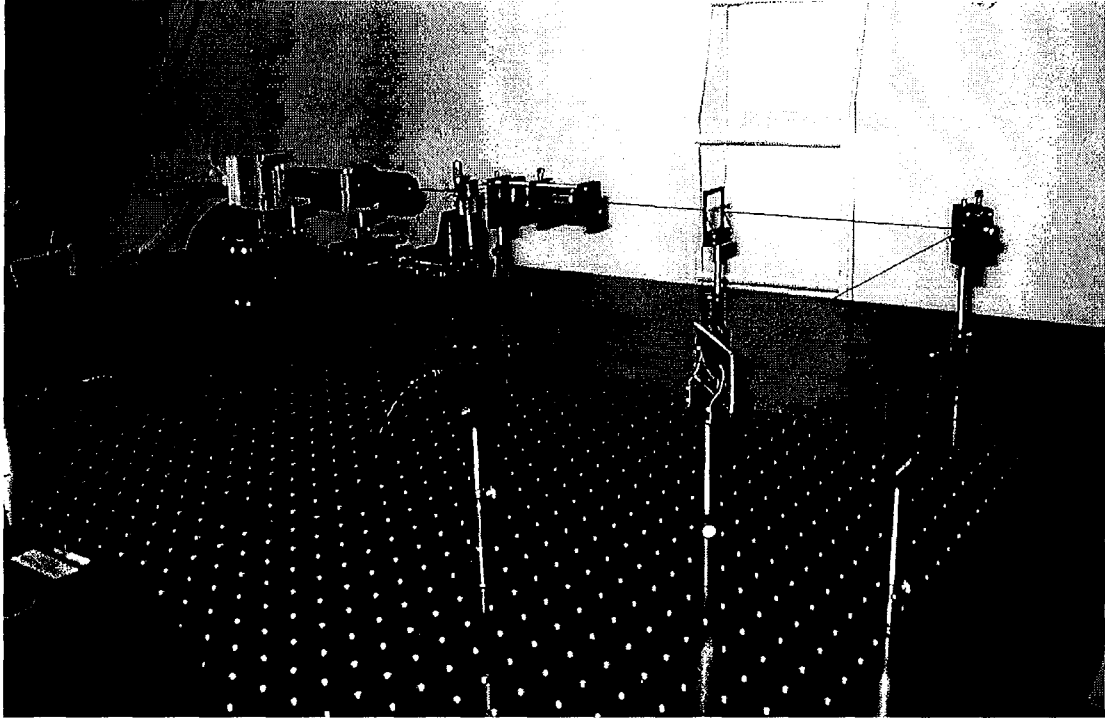
Appendix A

Figure A.1 Transmission set-up.